# Coastal Flood Vulnerability and Spatial Risk Assessment for Small Island Urban of Cat Ba Town, Northern Vietnam

**Phi, N. Q.,[1] Hoa, P. T. M.,[1,2*] Tuan, T. A.[3] and Cuc, N. T.[1]**
[1]Hanoi University of Mining and Geology, Hanoi, Vietnam
E-mail: phanthimaihoa@humg.edu.vn, ORCID ID: 0009-0002-7129-2170
[2]Graduate University of Science and Technology, Vietnam Academy of Science and Technology, Vietnam
[3]Institute of Earth Sciences, Vietnam Academy of Science and Technology, Vietnam
**Corresponding Author*

**DOI: https://doi.org/10.52939/ijg.v21i10.4537**

**Abstract**
*This study develops an integrated geospatial framework to assess coastal flood vulnerability in Cat Ba town, northern Vietnam. A binary flood inventory was generated from Sentinel-1 SAR imagery, while indicators describing the built environment were extracted from Google Earth and topographic datasets. Flood susceptibility was modeled with three decision tree algorithms: Classification and Regression Tree (CART), J48 and Reduced Error Pruning Tree (REPTree). Model performance was evaluated using the overall accuracy, AUC and Cohen's Kappa. To capture the spatial distribution of built environment exposure, a Built Environment Vulnerability Index (BEVI) was developed using the AHP-based approach. The BEVI composes 05 indicators, including built-up area density, road network density, building height, site elevation and distance to major infrastructures. The composite flood risk map, formed by overlaying BEVI and flood susceptibility outputs, revealed that low-lying areas near the town center and harbor are highly prone to flooding. Among the tested models, CART achieved the best performance, with 94.84% accuracy, an AUC of 0.925 and a Kappa value of 0.874. The resulting risk map offers a practical tool for land-use zoning, drainage planning, and emergency management, directly supporting the 2021–2030 Vietnamese national strategy for disaster prevention and climate adaptation. In particular, targeting the high-BEVI zones for adaptation will help fulfill the strategy's goal of proactive flood mitigation and climate adaptation.*

**Keywords:** Built Environment Vulnerability Index, Cat Ba Town, Decision Tree Models, Risk Assessment, Urban Flood Vulnerability

## 1. Introduction

Flooding is among the most pervasive natural hazards globally, presenting persistent threats to infrastructure, economic development and human livelihoods. The risks associated with flooding have intensified due to shifting climatic patterns and rapid urban expansion, especially in low-lying and insular settlements where geomorphological constraints limit adaptation capacity [1]. Vietnam is rated among the most flood-prone countries in the world, and its 2021–2030 National Strategy for Disaster Prevention and Control explicitly emphasizes proactive flood mitigation, climate adaptation, and loss reduction [2]. Cat Ba town, located on the southwestern edge of Cat Ba Island in northern Vietnam, exemplifies this dynamic. The town lies within a karstic coastal landscape that is both ecologically sensitive and increasingly urbanized, thereby exacerbating its vulnerability to pluvial and fluvial flooding.

Despite a growing body of research on flood susceptibility and vulnerability in Vietnam and other coastal regions [3] and [4], few studies have explicitly focused on small island urban settings where rapid tourism-driven urbanization intersects with complex karstic terrain [5]. Existing works either emphasize hydrodynamic simulations that require dense in-situ data [6] or concentrate on socio-economic indicators without accounting for geomorphological constraints [7] and [8]. This creates a critical research gap in developing a transferable, data-efficient framework that simultaneously captures flood hazard dynamics and built-environment vulnerability for small insular towns like Cat Ba.

Addressing this gap is essential for tailoring adaptation strategies under limited-data conditions and accelerating local climate-resilience planning [4] and [9].

Traditional flood assessments often focus exclusively on either hazard intensity or socioeconomic vulnerability. However, in the context of Cat Ba, where the natural and anthropogenic factors interact in complex ways, an integrated and spatially explicit approach is essential. Geographic Information Systems (GIS) combined with machine learning (ML) techniques provide a robust analytical framework for integrating heterogeneous datasets and capturing the nonlinear relationships that characterize flood dynamics [3] and [10]. Recent studies have further emphasized the strength of ML - GIS integration in flood modeling, particularly in coastal and insular environments where traditional hydrodynamic models are limited by data availability and topographic complexity [4] and [11].

Among the various available algorithms, decision tree classifiers, particularly the Classification and Regression Tree (CART), J48 (C4.5) and Reduced Error Pruning Tree (REPTree), offer several notable advantages. These models are capable of processing both categorical and continuous variables without requiring extensive preprocessing. In addition, they produce transparent, rule-based outputs that enhance interpretability and support stakeholder engagement. Decision trees have been shown to perform well in flood risk studies due to their ability to identify threshold-based relationships among predictors [9] and [12]. Furthermore, they are computationally efficient and remain reliable even when applied to datasets that are incomplete or affected by noise [13][14] and [15]. Recent applications have validated their robustness across diverse geographies, from Morocco [4] to South and Southeast Asia [16][17] and [18], confirming their utility in high-resolution, stakeholder-oriented flood modeling.

In parallel, vulnerability assessment using spatial indicators has gained momentum through composite indices such as the Built Environment Vulnerability Index (BEVI) [7]. This index enables the integration of infrastructure-based risk factors, including building height, road network density, built-up area ratio, building site elevation and proximity to major roads [8]. These factors are weighted using the Analytic Hierarchy Process (AHP) as proposed by Saaty (1980) [19] and further refined in subsequent applications [20] and [21]. Studies conducted by [6] and [22] successfully employed vulnerability indices derived from AHP in combination with machine learning models to map flood-prone zones in Vietnam.

Building on this foundation, the present study proposes a hybrid flood vulnerability assessment model for Cat Ba town that combines decision tree classifiers (CART, J48 and REPTree) with BEVI constructed through AHP. The flood susceptibility maps derived from machine learning are overlaid with spatial vulnerability layers to produce a composite flood risk map. This integrated framework not only captures hydrological hazards but also reflects the urban morphology and infrastructure sensitivity of the study area. The findings are expected to offer actionable insights for local planners and policymakers, particularly in identifying critical flood-prone zones and prioritizing adaptation investments. Moreover, the replicable nature of this methodology may be applicable to other small island towns in Southeast Asia facing similar challenges from hydrometeorological extremes and rapid urban growth.

## 2. Study Area

This study focuses on Cat Ba town, a compact coastal urban area located on the southeastern coast of Cat Ba Island, Special Administrative Zone of Hai Phong City, northern Vietnam in Figure 1. The town is framed by steep limestone hills and narrow coastal plains, creating a terrain susceptible to rapid surface runoff [5]. The town's NW-SE structural range contributes to its susceptibility to flooding. The regional fault lines, along which the town is situated, may disrupt natural water flow by forming channels that direct rainwater into residential and commercial zones. The interaction of these geological features with rising sea levels and frequent storm surges heightens the vulnerability of the town's infrastructure to both inland and coastal flooding. In particular, the fault zones often trap water, leading to longer periods of inundation after heavy rainfall, which further strains the already overwhelmed drainage system. Cat Ba town lies within a humid tropical monsoon zone, with intense rainfall and typhoons occurring between May and October. During Typhoon Prapiroon in July 2024, Cat Hai District recorded 150-200mm of rainfall in 24 hours, causing severe inundation [23]. Low elevation, dense construction and limited drainage infrastructure have intensified flood risk. As a result, Cat Ba town provides a representative case for assessing flood hazard and built environment vulnerability in rapidly urbanizing island towns in the area.

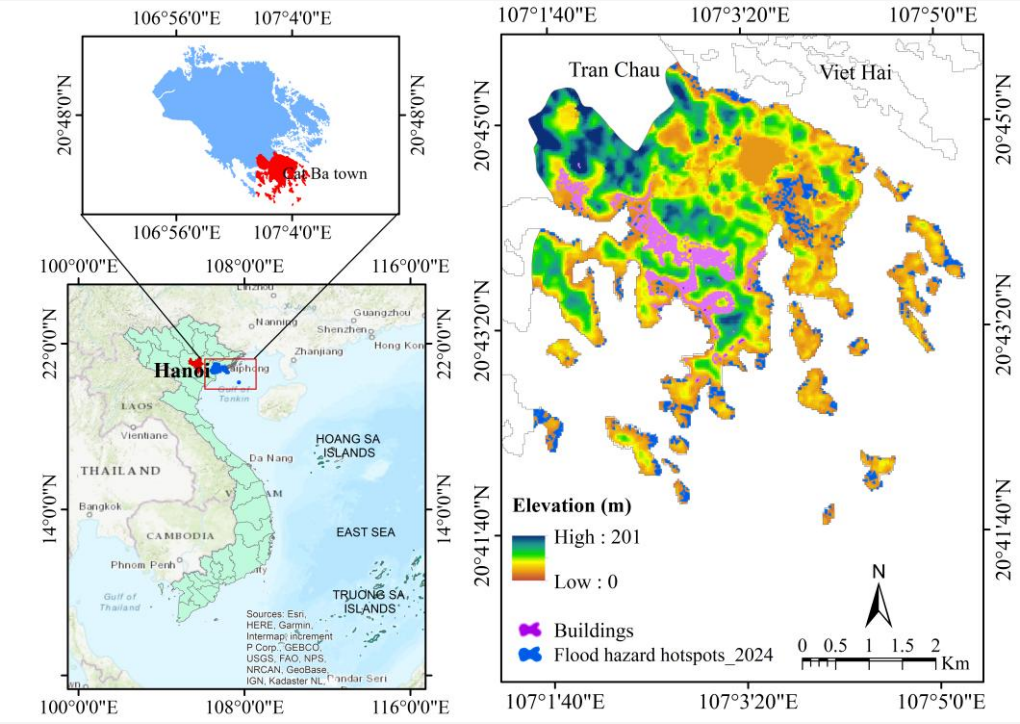


**Figure 1**: Location and topography of Cat Ba town

## 3. Methods and Data

*3.1 Methods*

The methodology integrated machine learning-based flood susceptibility mapping with a built environment vulnerability assessment to identify high-risk zones requiring adaptation interventions. Figure 2 presents the overall framework of the proposed approach.

*3.1.1 Flood hazard mapping using decision trees (CART, J48, REPTree)*

Flood hazard susceptibility on Cat Ba Island was modeled using three decision tree algorithms: Classification and Regression Trees (CART), J48 and REPTree. These methods were chosen for their efficiency, ability to capture complex non-linear relationships and ease of interpretation. Each algorithm recursively partitions the input data based on optimal split thresholds, forming a tree of decision rules that distinguish flood occurrence from non-occurrence.

Flood records (flooded and non-flooded locations) were compiled with nine flood-conditioning factors (elevation, slope, distance to rivers, etc.). The dataset was randomly split into 66% for training and 34% for testing, following standard practice. Model implementation used the Weka software, which provides robust versions of the CART, J48 and REPTree algorithms. This two-to-one division provided a sufficiently large sample to capture complex non-linear relationships while preserving an ample testing set for an unbiased assessment of predictive skill, a ratio widely adopted in flood and landslide susceptibility research [16] and [20]. Each the CART, J48, and REPTree was trained on the 66 % subset to calibrate optimal splitting rules and pruning parameters, and subsequently evaluated on the unseen 34 % subset to derive accuracy, sensitivity, specificity, F1-score, Cohen's Kappa, RMSE, and AUC-ROC. This design ensures a transparent and reproducible assessment of model generalization and underpins the reliability of the resulting flood-hazard maps.

CART builds a binary decision tree by selecting splits that minimize impurity. For classification, it uses the Gini impurity criterion to choose the best split at each node. The CART model applied cost-complexity pruning to avoid overfitting, cutting off branches that added complexity without improving prediction accuracy. The pruning parameter (complexity cost) was tuned via cross-validation, resulting in a simplified tree that generalizes well.

J48 is a decision tree classifier for Java implementation based on the C4.5 algorithm, which was developed by Ross Quinlan in 1993 [15]. C4.5 itself is an extended version of the earlier ID3 algorithm to handle continuous attributes by finding optimal threshold splits [15].

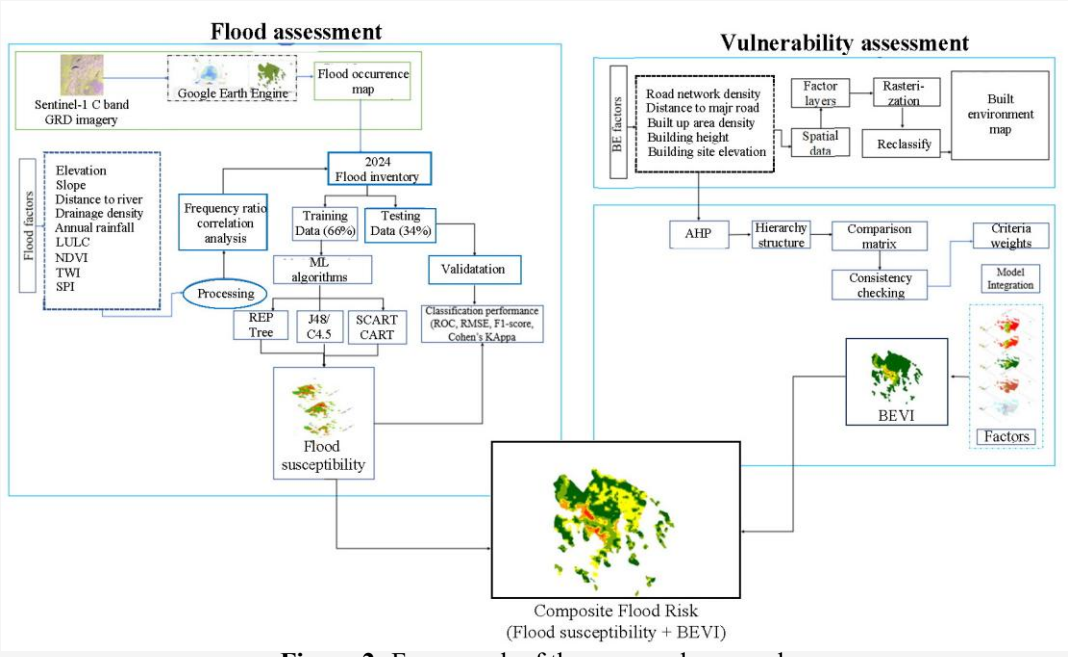


**Figure 2***:* Framework of the proposed approach

It uses the gain ratio (a normalized information gain) as its splitting metric, which avoids the bias of information gain toward attributes with many values. The Weka implementation (J48) prunes the initial tree using a confidence factor of 0.25, removing any branch that does not significantly improve classification accuracy. This produces a concise decision tree model (e.g. rules might involve elevation and distance-to-river thresholds) that is both accurate and interpretable.

REPTree is a fast decision tree learner in Weka that uses information gain for splitting and applies reduced-error pruning. It only sorts numeric attributes once and prunes using a separate validation subset, which makes it computationally efficient. As a result, REPTree typically produces a slightly simpler tree than J48 and is well-suited for large datasets or scenarios requiring quick modeling. After training, each decision tree was applied to the entire study area on a 30m grid to produce flood susceptibility maps. Each grid cell received a flood susceptibility score (probability) based on the model's classification. These continuous scores were normalized into a Flood Hazard Index and then classified into qualitative hazard levels (low, moderate, high) for visualization. The categorized flood hazard maps allow easy identification of high-risk zones versus lower-risk areas across Cat Ba town.

The importance of each conditioning factor was assessed by examining its frequency and hierarchical position within the decision tree structures. Across all three models, elevation and distance to rivers consistently emerged as the most influential variables, frequently appearing near the root nodes. These findings align with prior studies highlighting proximity to rivers and low-lying terrain as key determinants of flood susceptibility [24].

*3.1.2 Built environment vulnerability mapping using AHP*

The vulnerability of the built environment on Cat Ba town was evaluated using a Multi-Criteria Decision Analysis (MCDA) framework, specifically employing the Analytic Hierarchy Process (AHP). AHP is a widely recognized method for structuring complex decision problems into a hierarchical model comprising goals, criteria and alternatives [19] and [25]. Its application in flood risk assessment has become increasingly prominent due to its ability to systematically incorporate expert knowledge while providing a transparent and reproducible weighting scheme for contributing factors [26]. In the present study, the primary objective of the AHP framework was to identify areas exhibiting higher levels of built environment vulnerability to flood hazards. Five spatial indicators, which represent infrastructure density, physical exposure and structural characteristics, were selected based on prior studies and the availability of data in the area. These criteria were chosen for their critical roles in representing asset concentration, infrastructural connectivity and physical exposure, all of which significantly influence flood-induced impacts [27] and [28].

To establish the relative importance of the selected criteria, a panel of disaster risk management experts was convened to perform pairwise comparisons following the Saaty 1 to 9 fundamental scale [19]. Each expert independently evaluated the comparative importance of each pair of criteria in contributing to flood vulnerability. The individual assessments were subsequently aggregated using the geometric mean method to synthesize a consensus matrix. The consistency ratio (CR) of the final matrix was computed and yielded a value of 0.05, indicating a high level of internal consistency and logical coherence among expert judgments, which is well below the accepted threshold of 0.10) [19].

The Built Environment Vulnerability Index (BEVI) was then calculated by integrating the normalized values of the selected criteria through a weighted linear combination. The computed BEVI scores ranged from 0 to 1, with higher values indicating greater vulnerability of the built environment to flooding. To support interpretation and guide policy formulation, the BEVI map was subsequently classified into five qualitative vulnerability categories: Very Low, Low, Moderate, High and Very High. The Jenks natural breaks optimization method was employed for this classification to ensure meaningful division of vulnerability levels based on inherent data distribution [29].

*3.1.3 Model evaluation and validation*

*Sensitivity (SST):* Sensitivity quantifies the model's capability to accurately detect actual flood occurrences (true positives) among all observed flood cases [16] and [20]. It is computed in Equation 1 as:

$$SST = \frac{TP}{TP + TN}$$

Equation 1

Where: *TP* represents True Positives (flood correctly identified). *FN* denotes False Negatives (flood misclassified as stable areas). A higher sensitivity reflects a stronger ability of the model to detect hazardous zones, thereby minimizing overlooked landslide-prone areas.

*Specificity (SPF):* Specificity assesses the model's effectiveness in correctly classifying stable areas (true negatives) out of all actual non-landslide cases [16][30] and [31], calculated in Equation 2 as:

$$SPF = \frac{TN}{TN + FP}$$

Equation 2

Where: *TN* is True Negatives (correctly predicted stable zones); *FP* is False Positives (stable zones incorrectly classified as flood). This metric indicates the model's ability to avoid false alarms by correctly identifying areas without flood risk.

*Accuracy (ACC):* Accuracy measures the proportion of total correct predictions (including both flood and non-flood classes) relative to the entire dataset [31]. Accuracy is expressed in Equation 3.

$$ACC = \frac{TP + TN}{TP + TN + FP + FN}$$

Equation 3

Although widely used, accuracy alone may not sufficiently reflect model performance, especially when dealing with class-imbalanced data.

*F1-Score:* The predictive performance of each model was evaluated systematically on the independent testing subset. For classification tasks, evaluation metrics included *Accuracy*, *Precision*, *Recall* and the *F1-score*. The *F1-score*, representing the harmonic mean of *Precision* and *Recall* [32], was calculated in Equation 4 following as:

$$F1 = 2 \times \frac{Precision \times Recall}{Precision + Recall}$$

Equation 4

Where *Precision* and *Recall* are further defined in Equations 5 and 6, respectively:

$$Precision = \frac{TP}{TP + FP}$$

Equation 5

$$Recall = \frac{TP}{TP + FN}$$

Equation 6

Here, *TP* denotes true positives, *FP* false positives and *FN* false negatives. The *F1-score* thus provides a balanced measure of a model's performance by accounting for both false positives and false negatives, and is particularly critical in cases where class distributions are imbalanced, such as in vulnerability classifications.

Predictive accuracy can also be quantified through *Mean Squared Error (MSE), Mean Absolute Error (MAE)* and the *Coefficient of Determination ($R^2$)*. The $R^2$ metric is calculated as shown in Equation 7.

$$R^2 = 1 - \frac{\sum_{i=1}^{n}(y_i - \hat{y}_i)^2}{\sum_{i=1}^{n}(y_i - \bar{y}_i)^2}$$

Equation 7

Where $y_i$ are the observed values, $\hat{y}_i$ are the predicted values and $\bar{y}$ is the mean of the observed values.

To ensure model stability and to detect potential overfitting, the mean and standard deviation of each performance metric were reported across ten cross-validation folds. In addition to quantitative evaluation, model interpretability was assessed by analyzing the structure of the resulting decision trees. Attributes appearing near the root nodes were identified as critical predictors, offering substantive insights into how socioeconomic, structural and exposure factors shape built environment vulnerability under natural hazard events.

*Cohen's Kappa (K):* Cohen's Kappa evaluates the degree of agreement between predicted classifications and actual observations while adjusting for chance agreement [31]. *Cohen's Kappa (K)* is computed following Equation 8.

$$K = \frac{P_p - P_{exp}}{1 - P_{exp}}$$

Equation 8

Where $P_p$ is the observed agreement proportion; $P_{exp}$ is the expected agreement by random chance. Values closer to 1 imply strong agreement, whereas values near 0 indicate agreement equivalent to random classification.

*Root Mean Square Error (RMSE)* is defined in Equation 9: *RMSE* quantifies the average magnitude of prediction errors, thus providing insight into the model's precision [16]:

$$RMSE = \sqrt{\frac{\sum_{i=1}^{N}(X_P - X_a)^2}{N}}$$

Equation 9

Where $N$ is the sample size; $X_p$ are model predictions; $X_a$ are actual observed values.

Lower RMSE values indicate greater predictive precision, highlighting the model's capability to generate estimates with minimal deviation from actual observations. The AUC-ROC measures a model's ability to distinguish between positive and negative classes, with values ranging from 0 to 1. An AUC value of 1 denotes a perfect classifier with complete separation of classes, whereas a value of 0.5 indicates performance no better than random guessing. Values below 0.5 suggest that the model performs worse than random classification. Together, RMSE and AUC-ROC provide comprehensive insights into both the accuracy and discriminatory capacity of the models evaluated in this study.

### *3.2 Data Used*

#### *3.2.1 Flood hazard factors*

Flood susceptibility is strongly influenced by the underlying terrain, surface morphology and climatic factors from previous studies [4] and [16]. Based on the field observations and the availability of data, nine influence factors were selected for flood hazard modeling in Table 1 and Figure 3. Topographic attributes, including slope and elevation, are fundamental to controlling water movement and accumulation. Gentle slopes and low elevations favor water stagnation and accumulation, whereas steeper slopes facilitate rapid runoff [22][32] and [33]. Topographic wetness index (TWI) and stream power index (SPI) offer advanced insights into hydrological behavior. TWI quantifies the potential for water accumulation based on upslope contributing area and slope, making it particularly relevant for identifying saturated zones in Cat Ba's karst valleys and closed depressions [34][35] and [36]. Meanwhile, SPI reflects the erosive energy of surface flows, essential for detecting flash flood pathways in the island's steep and confined channels [16]. Together, these indices refine the model's capacity to differentiate between areas subject to ponding floods and areas exposed to high-energy runoff events.

Distance to rivers (DRi) is a classic predictor of flood hazard, as proximity to water channels directly influences inundation likelihood [32]. Drainage density (DD), representing the total length of streams per unit area, integrates the effects of terrain, geology and rainfall on runoff concentration [32]. Land use and land cover (LULC) play a pivotal role in modulating runoff generation and infiltration capacity, thereby influencing flood occurrence. Numerous studies have shown that impervious surfaces such as roads and buildings enhance surface runoff, while vegetated areas mitigate flood risks by promoting infiltration [16] and [22]. Rainfall is the primary climatic driver of flooding, especially in tropical monsoon environments like Cat Ba Island, where intense and short-duration rainfall events are common [4][32] and [37]. Finally, the normalized difference water index (NDWI) derived from remote sensing imagery enhances the modeling framework by capturing persistent surface water presence and soil moisture conditions [38].

**Table 1:** Summary of flood hazard and vulnerability factors with data sources and references

| Factor | Data Source | Description |
|---|---|---|
| Elevation | Topographic maps (1:10.000 scale) | Raster elevation values (DEM) used directly |
| Slope | Topographic maps (1:10.000 scale) | Derived from DEM using GIS slope tool |
| Distance to river (DRi) | OpenStreetMap (OSM) | GIS Euclidean distance from each cell to nearest river |
| Drainage density (DD) | OpenStreetMap (OSM) | Total stream length per area (GIS hydro tools) |
| Rainfall (annual) | CHIRPS daily rainfall dataset ("UCSBCHG/CHIRPS/DAILY") | Interpolated from average rainfall of 2024 in ArcGIS |
| Land use and land cover (LULC) | Google Dynamic World V1 (Sentinel-2) | Mode compositing of annual 2021 classification, 10m resolution |
| Topographic Wetness Index (TWI) | Topographic maps (1:10.000 scale) | TWI = ln(As / tan(β)) from flow accumulation (As) and slope (β) |
| Stream Power Index (SPI) | Topographic maps (1:10.000 scale) | SPI = As*tan(β) (where as is the local upslope catchment area draining through a specific pixel (often in square meters) and β is the local slope gradient (in degrees or radians)) |
| Normalized Difference Water Index (NDWI) | Sentinel-2 imagery of 2024 | Computed from green and near-infrared bands to highlight water bodies in GEE |
| **Flood inventory** | Sentinel-1 SAR images | Change detection (pre–post backscatter difference + threshold) |

**Table 2:** BEVI indicators and sources

| No. | Factors | Data Source | Description | References |
|---|---|---|---|---|
| 1 | Road Network Density (RND) | OpenStreetMap (OSM) | Total road length per km² (connectivity measure) | [39] |
| 2 | Distance to Major Roads (DMR) | OpenStreetMap (OSM) | Euclidean distance to main transportation corridors | [40] |
| 3 | Built-up Area Density (BAD) | Google Earth + Field Verification | Ratio of impervious surfaces over area; delineated from satellite images | [41] |
| 4 | Building Height (BH) | Google Earth + Field Survey | Estimated height of buildings interpreted visually and confirmed in field | [42] |
| 5 | Building Site Elevation (BSE) | Topographic maps (1:10.000 scale) | Surface elevation at building locations | [16] |

*3.2.2 Built environment vulnerability factors*

The Built Environment Vulnerability Index (BEVI) was generated based on five spatial indicators: road network density (RND), distance to major roads (DMR), built-up area density (BAD), building height (BH) and building site elevation (BSE) (Table 2 and Figure 4). Road network density (RND) reflects the extent of impervious surfaces while also shaping mobility and evacuation potential during flooding events. Densely connected road systems have been found to exacerbate surface runoff and influence flood exposure patterns [43]. Distance to major roads (DMR) is included based on evidence that such roads often incorporate engineered drainage infrastructure; proximity to these corridors can facilitate more effective runoff diversion and reduce local flooding severity [44]. Built-up area density (BAD) represents impervious cover, a widely recognized factor in urban flood generation by decreasing infiltration and increasing surface flow accumulation [39]. Building height (BH) influences flood impact levels, as low-rise structures are more susceptible to ground-level inundation compared to elevated multi-storey buildings [45].

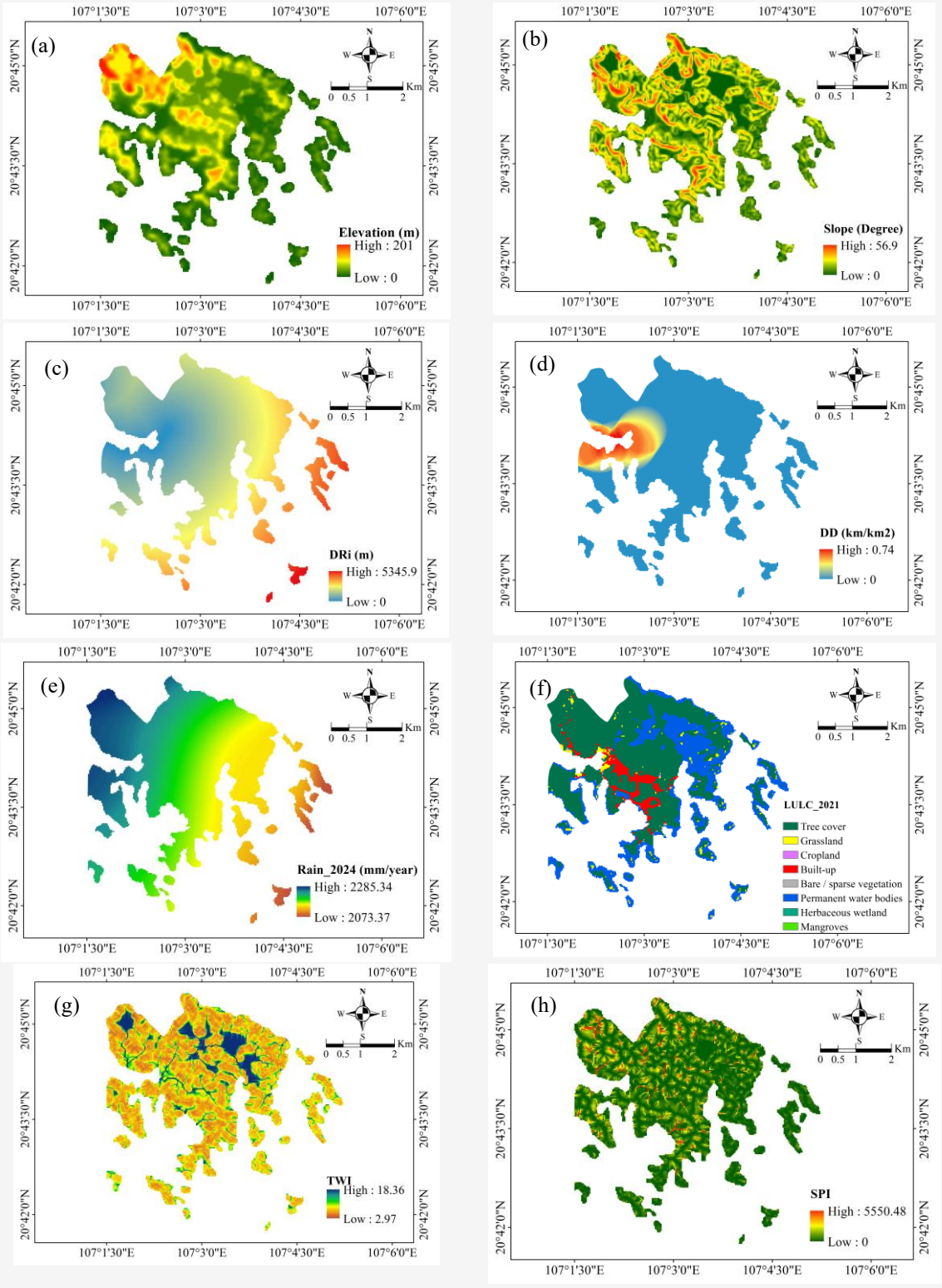


**Figure 3**: Flood Factors: (a) elevation, (b) slope, (c) distance to rivers, (d) drainage density, (e) rainfall, (f) land use land cover, (g) topographic wetness index, (h) stream power index, (i) normalized difference water index and (j) inventory map of flood 2024 (Continue next page)

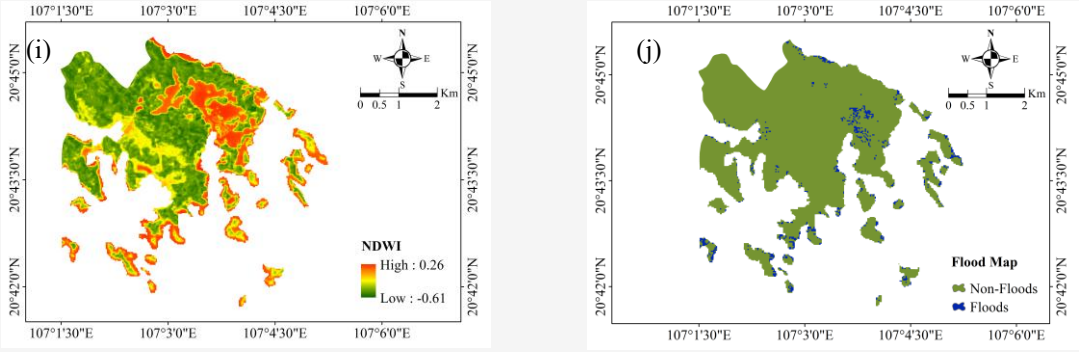


**Figure 3**: Flood Factors: (a) elevation, (b) slope, (c) distance to rivers, (d) drainage density, (e) rainfall, (f) land use/land cover, (g) topographic wetness index, (h) stream power index, (i) normalized difference water index and (j) inventory map of flood 2024 (Continue from previous page)

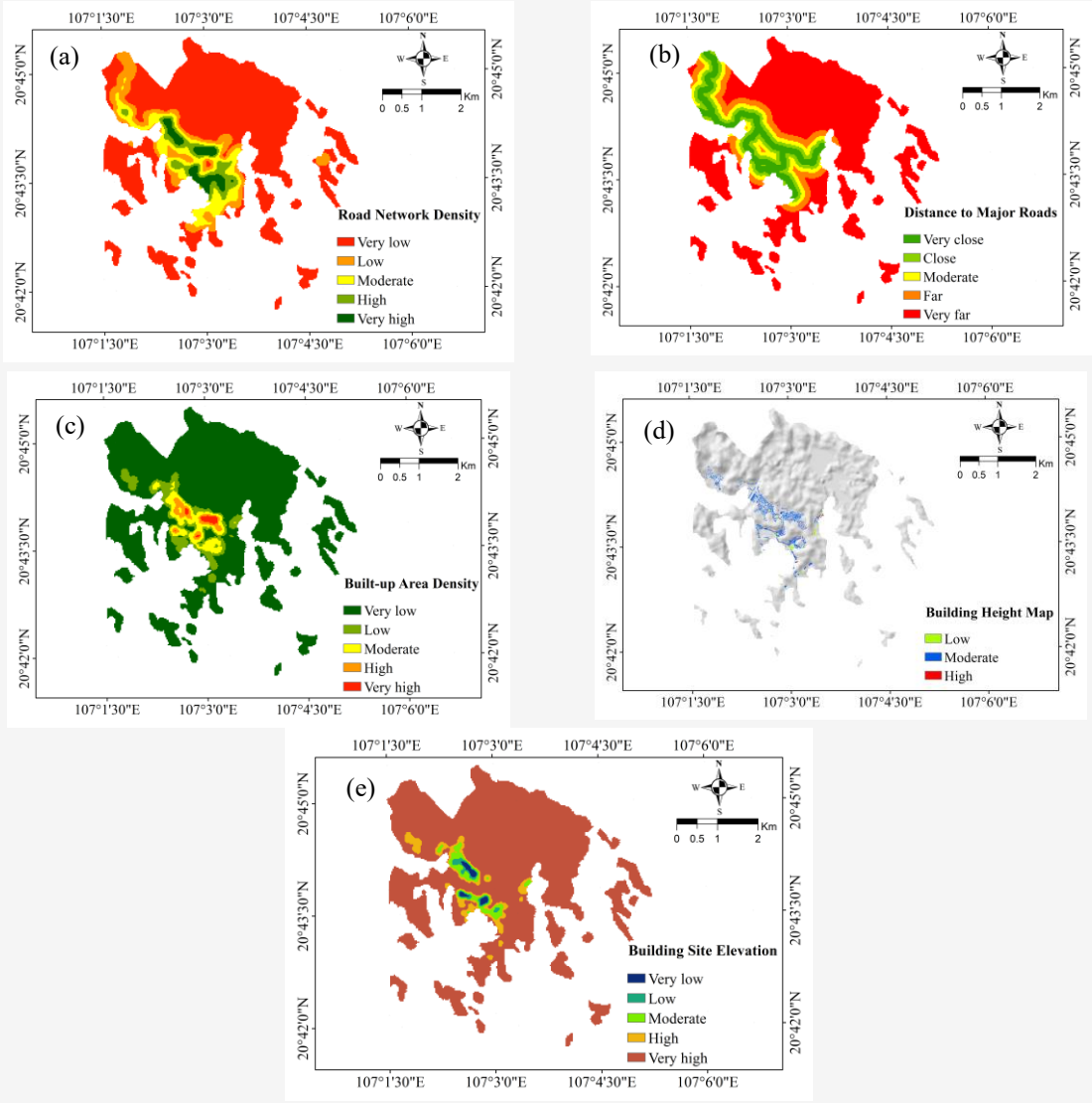


**Figure 4**: Built Environment factors: (a) road network density, (b) distance to major roads, (c) built-up area density, (d) building height map, (e) building stie elevation

Finally, building site elevation (BSE) fundamentally governs flood hazard exposure, with lower elevations posing significantly greater inundation risk [45]. These five indicators were selected based on their frequent identification as significant determinants of urban flood vulnerability in recent literature [44] and [45]. These variables reflect both the concentration of exposure and the structural sensitivity of urban infrastructure, especially in flood-prone lowlands.

Building height and built-up area density were derived through visual interpretation of high-resolution imagery from Google Earth combined with in-situ field surveys, allowing accurate delineation of structural characteristics and urban form in the study area. Road network data and major road locations were extracted from OpenStreetMap (OSM), while elevation data was obtained from topographic maps of the study area at 1:10.000 scale, providing consistent topographic context for site-specific vulnerability mapping.

This integrated approach aligns with international practices for urban flood risk modeling in data-limited environments [41] and [42], ensuring both methodological rigor and contextual specificity. A binary flood-inventory map of 2024 was generated in Google Earth Engine (GEE) using Sentinel-1 C-band SAR Ground Range Detected (GRD) imagery, labeling flooded (1) versus non-flooded (0) pixels [46] and [47]. This inventory was compiled from pre- and post-flood Sentinel-1 acquisitions. The pre-flood reference comprised images from January 1 to April 30, 2024 and the post-flood imagery spanned November 1 to December 30, 2024, capturing conditions after heavy rainfall. The Sentinel-1 scenes were filtered to vertical-vertical (VV) polarization and interferometric wide-swath (IW) mode to enhance surface-water detection under all-weather, day-and-night conditions [47]. Using these filtered images, 18,067 reference points were extracted (795 flooded; 17,272 non-flooded) by verifying radar backscatter changes against high-resolution optical imagery and visual inspection. Non-flooded samples were deliberately chosen from areas unaffected by flooding, landslides, or other disturbances to ensure data integrity. Finally, the dataset was randomly partitioned (66% training, 34% testing) and used to build three decision-tree classifiers (REPTree, J48 and CART) in the WEKA environment for subsequent flood-susceptibility modeling.

## 4. Result

### *4.1 Flood Hazard Mapping Results*

Among the evaluated decision tree models, the CART algorithm demonstrated the most robust and balanced performance for flood susceptibility mapping in Cat Ba town. It achieved the highest overall accuracy (94.84%) and *F1-score* (0.947), alongside a strong Cohen's Kappa (0.8744), indicating excellent agreement with observed flood data in Table 3 and Figure 5. While REPTree recorded a slightly higher AUC (0.962) and sensitivity (0.976), its relatively lower specificity and Kappa coefficient suggest that it was less effective in distinguishing non-flooded areas. The J48 model underperformed across all metrics, with notably low specificity (0.414) and accuracy (69.91%). Given the urban and topographic complexity of Cat Ba, CART's superior balance between sensitivity and specificity makes it the most reliable model for operational flood hazard classification in this setting. These results are consistent with other flood-susceptibility studies in which decision-tree algorithms (such as CART) effectively delineated flood-prone areas [9].

This study presents an innovative flood susceptibility assessment for Cat Ba town, integrating Sentinel-1 SAR data with three machine learning models (REPTree, J48 and CART). Among analyzed predictors, NDWI and land use emerged as primary determinants of flood occurrence, significantly outperforming traditional topographic indices such as elevation, TWI and SPI. Elevated NDWI values consistently indicated high surface moisture and permanent water presence, directly correlating with observed inundation zones, aligning with recent studies highlighting NDWI's predictive strength [48] and [49]. Similarly, land-use classifications, particularly peri-urban and agricultural areas, exhibited heightened vulnerability due to impermeable surfaces and disrupted drainage systems, consistent with findings by [50].

**Table 3***:* Classification performance of CART, J48 and REPTree models for flood hazard mapping on Cat Ba town

| Model | Sensitivity | Specificity | Accuracy (%) | Precision | F1-score | Cohen's Kappa | RMSE | ROC-AUC |
|---|---|---|---|---|---|---|---|---|
| **REPTree** | 0.976 | 0.852 | 93.83 | 0.938 | 0.937 | 0.851 | 0.243 | 0.962 |
| **J48** | 0.824 | 0.414 | 69.91 | 0.685 | 0.690 | 0.251 | 0.432 | 0.713 |
| **CART** | 0.987 | 0.860 | 94.84 | 0.949 | 0.947 | 0.874 | 0.226 | 0.925 |

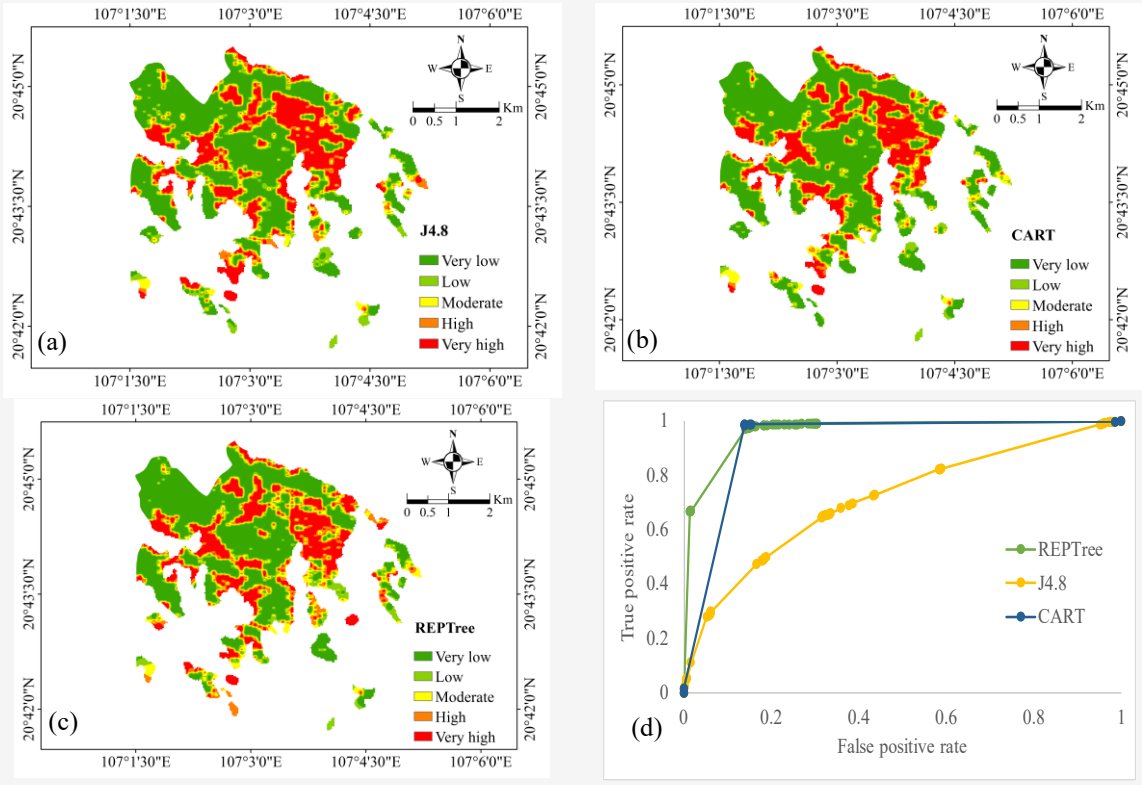


**Figure 5:** Flood Hazard maps of (a) J48, (b) CART and (c) REPTree; (d) ROC chart

**Table 4**: Decimal matrix of pairwise comparisons and criterion weights

| Criterion | BH | DMR | RND | BAD | BSE | Weight |
|---|---|---|---|---|---|---|
| **BH** | 1 | 0.33 | 0.2 | 0.14 | 0.33 | 0.049 |
| **DMR** | 3 | 1 | 0.33 | 0.2 | 0.5 | 0.098 |
| **RND** | 5 | 3 | 1 | 0.33 | 1 | 0.209 |
| **BAD** | 7 | 5 | 3 | 1 | 3 | 0.473 |
| **BSE** | 3 | 2 | 1 | 0.33 | 1 | 0.170 |
| **Sum** | 19 | 11.33 | 5.53 | 2.01 | 5.83 | |

Topographic factors, although traditionally influential, played secondary roles in predicting flood susceptibility on Cat Ba, emphasizing the greater relevance of hydrological conditions and anthropogenic alterations in this specific coastal setting. The CART model achieved the highest predictive accuracy (94.84%, K=0.87, AUC=0.925), effectively delineating critical flood-prone zones concentrated in low-lying western and semi-urban regions. Compared to conventional rainfall or DEM-based methodologies, this integrated SAR-driven machine-learning framework provided significantly improved spatial accuracy and practical utility [51].

*4.2 Built Environment Vulnerability Mapping Results*

The Built Environment Vulnerability Index (BEVI) is a composite indicator used to evaluate the exposure of urban areas to flood impacts. It integrates five spatial factors weighted by their relative importance using the Analytic Hierarchy Process (AHP) [52] and [53]. During the pairwise comparison process, experts evaluated the relative importance of each criterion using the fundamental Saaty scale, where values from 1 to 9 denote increasing dominance and their reciprocals indicate decreasing importance. The summarized comparison matrix is presented in Table 4. The assigned weights were: Built-up Area Density (47%), Road Network Density (21%), Building Site Elevation (17%), Distance to Major Roads (10%) and Building Height (5%) in Table 5. The Consistency Index (CI) and Consistency Ratio (CR) are calculated from the principal eigenvalue to confirm the logical coherence of expert judgments. The Consistency Index (CI) and Consistency Ratio (CR) were derived from the principal eigenvalue to evaluate the logical consistency of the expert assessments, and the calculated CR of 0.026, which

is below the accepted threshold of 0.1, demonstrates that the pairwise comparison matrix provides reliable and coherent judgments. BEVI was calculated through a weighted overlay of normalized spatial layers, resulting in a map that classifies vulnerability levels from very low to very high (Figure 6).

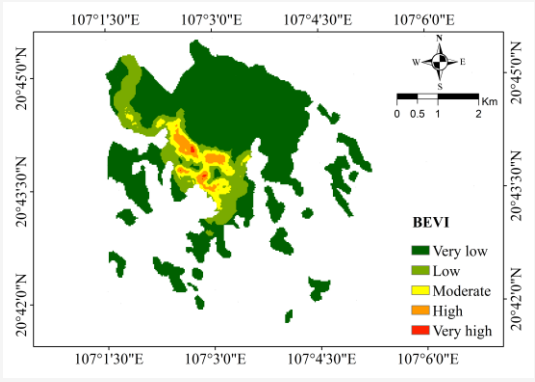


**Figure 6:** BEVI map of Cat Ba town

The index incorporates key dimensions of vulnerability, including exposure (e.g., dense development), sensitivity (e.g., low elevation or short buildings) and adaptive capacity (e.g., road accessibility). Higher BEVI values identify areas where flood impacts are likely to be more severe due to high exposure, high sensitivity, or limited access, and thus highlight priority zones for risk management.

The spatial distribution of BEVI values revealed a clear concentration of high vulnerability in the low-lying, densely developed core of Cat Ba town, particularly along the coastal frontage. This pattern was largely driven by exposure-related factors, with Built-up Area Density and Building Site Elevation exerting the most significant influence on the index. Meanwhile, Road Network Density and Distance to Major Roads contributed to more localized differentiation in vulnerability, particularly in outlying settlements with limited accessibility. Building Height, though assigned the lowest weight, offered additional nuance in areas characterized by uniform exposure but varied structural forms. Overall, the results underscore a spatially uneven pattern of vulnerability, with the urbanized coastal zone emerging as the most at-risk area. This highlights the critical need to manage urban expansion more cautiously in flood-prone zones and to implement resilient infrastructure and spatial planning strategies to mitigate future flood risks [54] and [55].

### *4.3 Composite Flood Risk Map*

The integration of the flood hazard map and the Built Environment Vulnerability Index (BEVI) map resulted in the development of a comprehensive flood risk map that reflects the combined effects of susceptibility and exposure in Figure 7.

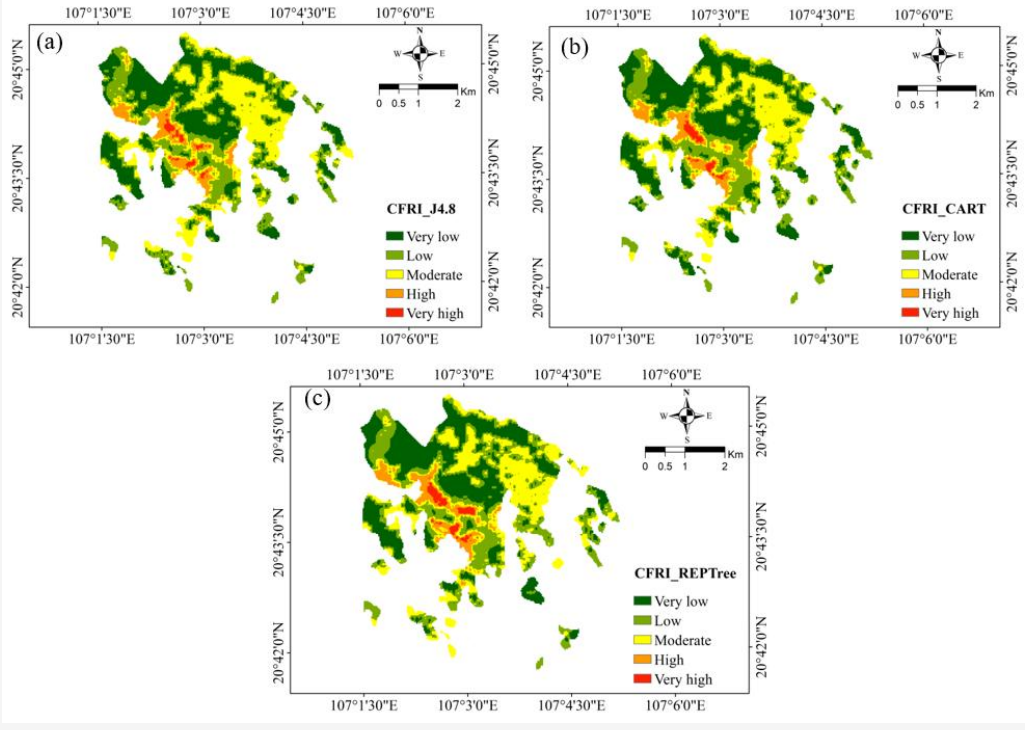


**Figure 7:** Classified maps of Flood risk zones using: (a) J48, (b) CART and (c) REPTree; (d) Flood conditions observed in Cat Ba town on July 2, 2024 (Continue next page)

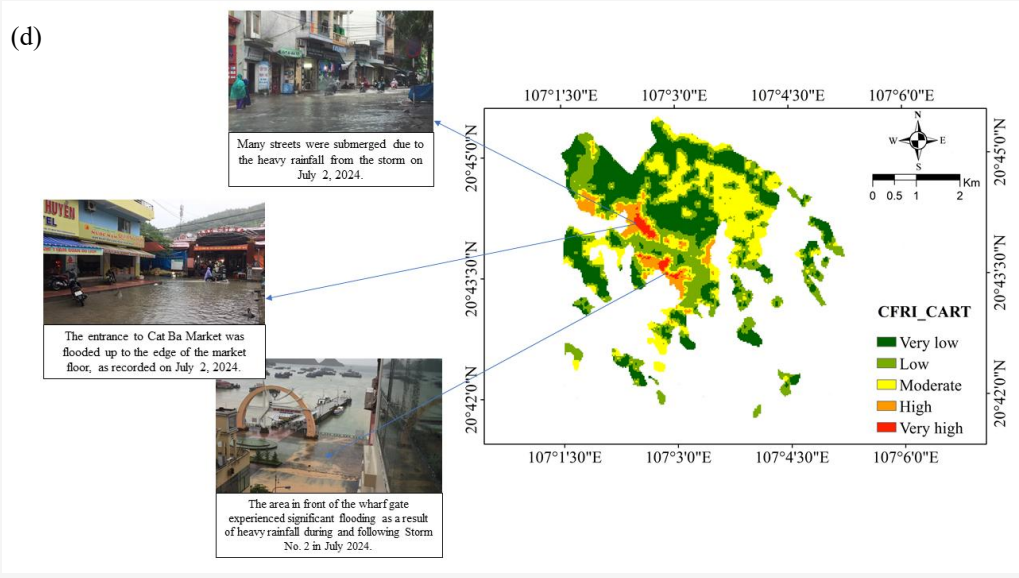


**Figure 7:** Classified maps of Flood risk zones using: (a) J48, (b) CART and (c) REPTree; (d) Flood conditions observed in Cat Ba town on July 2, 2024 (Continue from previous page)

Areas of highest risk correspond to zones where elevated flood hazard probabilities overlap with very high vulnerability, predominantly concentrated in the downtown and port regions of Cat Ba town. In these locations, the extensive presence of impervious surfaces and dense infrastructure substantially amplifies flood impacts, leading to pronounced flood risks. Conversely, the mountainous forested interiors, characterized by higher elevations and natural land cover, exhibit both low hazard levels and minimal built environment vulnerability, thus resulting in negligible flood risk. The most critical convergence of hazard and vulnerability is observed within the urbanized areas, whereas the natural upland zones remain largely resilient. This spatial pattern aligns with previous findings, such as those reported in Portugal, where high urban vulnerability sharply contrasted with the low vulnerability of surrounding agricultural areas [56]. Overall, the integrated analysis highlights that Cat Ba's town center and harbor precincts represent the principal flood-risk hotspots, while the outlying forested highlands are comparatively secure from flood impacts.

## 5. Discussion

The integration of the Built Environment Vulnerability Index (BEVI) with flood susceptibility maps generated from three decision tree models, including Classification and Regression Tree (CART), J48 and Reduced Error Pruning Tree (REPTree), provided a comprehensive spatial assessment of flood risk in Cat Ba town. Among the models, CART model achieved the best performance with an accuracy of 94.84%, a Kappa coefficient of 0.87 and an area under the curve (AUC) of 0.93. This model effectively delineated flood-prone zones, particularly in low-lying urban cores and coastal sectors [12] and [17].

A comparative evaluation of the three decision tree classifiers also offers insight into their operational characteristics. Although all models consistently identified the urban core and coastal areas as high-risk zones, their spatial granularity differed. The J48 model provided fine-scale outputs suited for micro-level interventions, whereas the CART model yielded broader patterns more applicable to regional planning. In contrast, the CART classifier balanced spatial precision with predictive accuracy, making it the most effective model overall. This result is consistent with other studies that have demonstrated the robustness and interpretability of tree-based algorithms in flood risk modeling [9] and [31]. While all three models identified similar high-risk areas, the CART model offered an optimal balance between predictive accuracy and spatial clarity. Its effectiveness reinforces the value of decision tree models when combined with contextual indicators like BEVI for urban flood risk assessment. The unique and complex terrain setting of the island poses significant flood risks for Cat Ba town. The underlying limestone geology of Cat Ba town further exacerbates the flood risk. Limestone karst formations are prone to erosion and dissolution, which leads to the development of extensive cave systems, sinkholes and fissures. While this gives the region its scenic beauty, it also reduces the natural

permeability of the soil. The poor permeability means that rainwater does not easily seep into the ground, causing surface runoff to accumulate rapidly during intense rainfall. This situation is especially problematic when the town experiences monsoonal rains, which are becoming more frequent and intense due to climate change, leading to flash floods and waterlogging in low-lying areas, especially the newly developed areas of Cai Gia urban area in the west and Tung Thu, Cat Co 1, 2, 3 beaches along the south eastern shore.

Validation using 2024 field survey data confirmed that frequently inundated areas, including the central market, ferry terminal access roads and harbor vicinity, aligned closely with zones of high BEVI and flood susceptibility (Figure 7d). These areas were marked by dense built-up structures, limited drainage and close proximity to major roads. Observations from local authorities further supported these findings and highlighted existing infrastructure deficiencies. This type of field validation has been endorsed by other empirical studies, reinforcing the robustness of combined modeling and ground verification approaches [18] and [57]. The town's drainage system, which was designed for a smaller, less developed population, is poorly equipped to handle the increasing volume of runoff generated by urbanization. With the rapid growth of infrastructure and the lack of adequate planning for stormwater management, many parts of Cat Ba town face frequent drainage blockages and slow water drainage, particularly along Cai Beo and Tung Dinh roads.

Another critical factor amplifying the flood risk in Cat Ba town is the low vegetation cover. Vegetation plays a key role in mitigating flood risk by absorbing rainwater, stabilizing soil and slowing down runoff. However, rapid urbanization in the region have resulted in the loss of large swaths of natural vegetation. The resulting barren landscapes reduce the land's capacity to absorb water, thereby increasing the volume and speed of surface runoff during heavy rains. Urban expansion, such as the SunGroup construction project, which is filling part of Lan Ha Bay, right in front of Cat Ba town, has also led to the construction of impermeable surfaces such as roads, public spaces and buildings, further hindering water absorption and contributing to flash flooding.

The composite flood risk maps corresponded well with historical flood events and known hydrological patterns. Unlike conventional models based solely on terrain or rainfall, this integrated approach captured the socio-physical dimensions of urban vulnerability. It offers practical value for spatial planning and disaster mitigation in small island towns, particularly under climate stress. Such integrative approaches are particularly relevant to small island towns, where flood risk is shaped not only by natural hazards but also by urban morphology and infrastructure limitations [58]. As a result, even moderate rainfall can lead to water accumulation, disrupting daily life and causing significant economic damage. The combination of Cat Ba's challenging topography, geologic instability, insufficient vegetation, rapid urbanization, and poorly managed drainage systems collectively elevates the flood risk, making it crucial to implement improved flood mitigation strategies in the region.

## 6. Conclusion

This study set out to evaluate coastal flood risk in Cat Ba Town by combining decision tree models for flood susceptibility with a Built Environment Vulnerability Index (BEVI). The research objective was to generate an operational flood-risk framework that captures both hydrological drivers and the spatial characteristics of the built environment to support local adaptation planning.

The results confirm that this objective has been achieved. Among the three decision tree classifiers, the CART model produced the most reliable flood-susceptibility surface, achieving an overall accuracy of 94.84 %, an AUC of 0.93, and a Kappa value of 0.87. When combined with the AHP derived BEVI, the resulting composite risk map accurately delineates the low-lying town centre and harbour areas as the most flood-prone zones, findings that were validated by field observations during the 2024 rainy season. The analysis further highlights how the town's rugged limestone topography, inadequate drainage capacity, and dense urban form interact to exacerbate flood hazards. By explicitly integrating structural indicators such as building density, road network connectivity, and site elevation, this approach provides a more detailed and nuanced representation of exposure and sensitivity compared with conventional topographic models. From a policy perspective, the flood-risk maps provide direct guidance for land-use zoning, drainage improvements, and emergency response planning. This guidance is consistent with Vietnam's National Strategy for Disaster Prevention and Climate Adaptation for the period 2021 to 2030. The findings also inform the tourism sector, a key economic driver on Cat Ba Island, by identifying safe sites and design parameters for new facilities.

Future research directions should focus on incorporating dynamic land use changes and climate projections to enhance the temporal sensitivity of the models. Additionally, expanding vulnerability assessments to integrate socio-economic indicators

would enable a more comprehensive understanding of flood risk across different community groups. Overall, the study demonstrates that integrating BEVI with interpretable machine-learning models provides a robust and transferable methodology for coastal flood-risk assessment in small island towns. This framework successfully fulfills the stated research objectives and delivers actionable knowledge for planners and decision makers seeking to balance rapid urbanization with climate resilience.

**Acknowledgements**
This research was funded by the Master, PhD Scholarship Programme of Vingroup Innovation Foundation (VINIF), code VINIF.2024.TS.109. We would like to thank the anonymous reviewers for their valuable comments, which significantly enhanced the quality of this publication.

**References**

[1] Lwasa, S., Seto, K. C., Bai, X., Blanco, H., Blanco, K. R., Kilkiş, S., Lucon, O., Murakami, J., Pan, J., Sharifi, A. and Yamagata, Y., (2022). Urban Systems and Other Settlements. In IPCC, 2022: Climate Change 2022: Mitigation of Climate Change. *Contribution of Working Group III to the Sixth Assessment Report of the Intergovernmental Panel on Climate Change*. Cambridge University Press, Cambridge, UK and New York, NY, USA. 861 – 952. https://doi.org/10.1017/9781009157926.010.

[2] Amirjalali, S., (2024). Climate Change Knowledge Portal. *The Scientific-Cultural Journal of Ecosphere*, Vol. 7(3), 77-82. https://ecosphersj.ut.ac.ir/article_100045.html?lang=en.

[3] Pham, B. T., Phong, T. V., Nguyen, H. D., Qi, C., Al-Ansari, N., Amini, A., Ho, L. S., Tuyen, Tr. T., Yen, H. P. H., Ly, H. B., Prakash, I. and Tien Bui, D., (2020). A Comparative Study of Kernel Logistic Regression, Radial Basis Function Classifier, Multinomial Naïve Bayes, and Logistic Model Tree for Flash Flood Susceptibility Mapping. *Water*, Vol. 12(1). https://doi.org/10.3390/w12010239.

[4] Mekkaoui, O., Morarech, M., Bouramtane, T., Barbiero, L., Hamidi, M., Akka, H. and Rengasamy, R. P. M., (2025). Unveiling Urban Flood Vulnerability: A Machine Learning Approach for Mapping High Risk Zones in Tetouan City, Northern Morocco. *Urban Science*, Vol. 9(3). https://doi.org/10.3390/urbansci9030070.

[5] Phuong, T. H., Cu, N. H., Thanh, T. D. and Van Dong, B., (2013). Geoheritage Values in the Cat Ba Islands, Vietnam. *Environmental Earth Sciences*, Vol. 70, 543-548. https://doi.org/10.1007/s12665-013-2619-1.

[6] Dung, N. B., Long, N. Q., An, D. T. and Minh, D. T., (2021). Multi-Geospatial Flood Hazard Modelling for a Large and Complex River Basin with Data Sparsity: A Case Study of the Lam River Basin, Vietnam. *Earth Systems and Environment,* Vol. 6, 715–731. https://doi.org/10.1007/s41748-021-00215-8.

[7] Borden, K. A., Schmidtlein, M. C., Emrich, C. T., Piegorsch, W. W. and Cutter, S. L., (2007). Vulnerability of US Cities to Environmental Hazards. *Journal of Homeland Security and Emergency Management*, Vol. 4(2). https://doi.org/10.2202/1547-7355.1279.

[8] Johnson, D., Blackett, P., Allison, A. E. and Broadbent, A. M., (2023). Measuring Social Vulnerability to Climate Change at the Coast: Embracing Complexity and Context for More Accurate and Equitable Analysis. *Water*, Vol. 15(19). https://doi.org/10.3390/w15193408.

[9] Antzoulatos, G., Kouloglou, I. O., Bakratsas, M., Moumtzidou, A., Gialampoukidis, I., Karakostas, A., Lombardo, F., Fiorin, R., Norbiato, D., Ferri, M., Symeonidis, A., Vrochidis, S. and Kompatsiaris, I., (2022). Flood Hazard and Risk Mapping by Applying an Explainable Machine Learning Framework Using Satellite Imagery and GIS Data. *Sustainability*, Vol. 14(6). https://doi.org/10.3390/su14063251.

[10] Mosavi, A., Ozturk, P. and Chau, K. W., (2018). Flood Prediction Using Machine Learning Models: Literature Review. *Water*, Vol. 10(11). https://doi.org/10.3390/w10111536.

[11] Dey, H., Shao, W., Moradkhani, H., Keim, B. D. and Peter, B. G., (2024). Urban Flood Susceptibility Mapping Using Frequency Ratio and Multiple Decision Tree-Based Machine Learning Models. *Natural Hazards*, Vol. 120(11), 10365-10393. https://doi.org/10.1007/s11069-024-06609-x.

[12] Chen, W., Hong, H., Li, S., Shahabi, H., Wang, Y., Wang, X. and Ahmad, B. B., (2019). Flood Susceptibility Modelling Using Novel Hybrid Approach of Reduced-Error Pruning Trees with Bagging and Random Subspace Ensembles. *Journal of Hydrology*, Vol. 575, 864-873. https://doi.org/10.1016/j.jhydrol.2019.05.089.

[13] Breiman, L., Friedman, J., Olshen, R. A. and Stone, C. J., (1984). Classification and Regression Trees (1st ed.). *Chapman and Hall/CRC*. https://doi.org/10.1201/9781315139470.

[14] Quinlan, J. R., (1986). Induction of Decision Trees. *Machine Learning,* Vol. 1(1), 81–106. https://doi.org/10.1023/A:1022643204877.

[15] Sharma, S., Agrawal, J. and Sharma, S., (2013). Classification through Machine Learning Technique: C4. 5 Algorithm Based on Various Entropies. *International Journal of Computer Applications*, Vol. 82(16), 20-27. https://doi.org/10.5120/14249-2444.

[16] Tehrany, M. S., Pradhan, B. and Jebur, M. N., (2013). Spatial Prediction of Flood Susceptible Areas Using Rule Based Decision Tree (DT) and a Novel Ensemble Bivariate and Multivariate Statistical Models in GIS. *Journal of Hydrology*, Vol. 504, 69-79. https://doi.org/10.1016/j.jhydrol.2013.09.034.

[17] Xing, Z., Lyu, G., Yao, Y., Liu, Z. and Zhang, X., (2025). Fine-Grained Analysis and Mapping of Urban Flood Susceptibility with Interpretable Machine Learning: A Case Study of Hefei, China. *Journal of Hydrology: Regional Studies*, Vol. 60. https://doi.org/10.1016/j.ejrh.2025.102501.

[18] Taromideh, F., Fazloula, R., Choubin, B., Emadi, A. and Berndtsson, R., (2022). Urban Flood-Risk Assessment: Integration of Decision-Making and Machine Learning. *Sustainability*, Vol. 14(8). https://doi.org/10.3390/su14084483.

[19] Saaty, T. L., (1990). The Analytic Hierarchy Process. *European Journal of Operational Research*, Vol. 48, 9-26.

[20] Hong, H., Panahi, M., Shirzadi, A., Ma, T., Liu, J., Zhu, A. X., Chen, W., Kougias, I. and Kazakis, N., (2018). Flood Susceptibility Assessment in Hengfeng Area Coupling Adaptive Neuro-Fuzzy Inference System with Genetic Algorithm and Differential Evolution. *Science of the Total Environment*, Vol. 621, 1124-1141. https://doi.org/10.1016/j.scitotenv.2017.10.114.

[21] Yilmaz, O. S., (2022). Flood Hazard Susceptibility Areas Mapping Using Analytical Hierarchical Process (AHP), Frequency Ratio (FR) And AHP-FR Ensemble Based on Geographic Information Systems (GIS): A Case Study for Kastamonu, Türkiye. *Acta Geophysica*, Vol. 70(6), 2747-2769. https://doi.org/10.1007/s11600-022-00882-9.

[22] Luu, C., Von Meding, J. and Kanjanabootra, S., (2018). Assessing Flood Hazard Using Flood Marks and Analytic Hierarchy Process Approach: A Case Study for the 2013 Flood Event in Quang Nam, Vietnam. *Natural Hazards*, Vol. 90, 1031-1050. https://doi.org/10.1007/s11069-017-3083-0.

[23] Typhoon Prapiroon Weakens, Leaving Nearly 3,900 Tourists Stranded on Cat Ba Island. *Asia News Network.* Available: https://asianews.network/typhoon-prapiroon-weakens-leaving-nearly-3900-tourists-stranded-on-cat-ba-island/ [Accessed: July 24, 2024].

[24] Al-Kindi, K. M. and Alabri, Z., (2024). Investigating the Role of the Key Conditioning Factors in Flood Susceptibility Mapping Through Machine Learning Approaches. *Earth Systems and Environment*, Vol. 8(1), 63-81. https://doi.org/10.1007/s41748-023-00369-7.

[25] Thammaboribal, P., Triapthti, N., and Lipiloet, S. (2025). Using of Analytical Hierarchy Process (AHP) in Disaster Management: A Review of Flooding and Landslide Susceptibility Mapping. *International Journal of Geoinformatics*, Vol. 21(4), 177–196. https://doi.org/10.52939/ijg.v21i4.4091.

[26] Mohd Rasu, M., Suhandri, H., Khalifa, N., Abdul Rasam, A., and Hamid, A. (2023). Evaluation of Flood Risk Map Development through GIS-Based Multi-Criteria Decision Analysis in Maran District, Pahang - Malaysia. *International Journal of Geoinformatics*, Vol. 19(10), 1–16. https://doi.org/10.52939/ijg.v19i9.2873.

[27] Cutter, S. L., Boruff, B. J. and Shirley, W. L., (2006). *Social Vulnerability to Environmental Hazards. In: Hazards Vulnerability and Environmental Justice*. Routledge. 115-132.

[28] Jongman, B., Ward, P. J. and Aerts, J. C., (2012). Global Exposure to River and Coastal Flooding: Long Term Trends and Changes. *Global Environmental Change*, Vol. 22(4), 823-835. https://doi.org/10.1016/j.gloenvcha.2012.07.004.

[29] Jenks, G. F. and Caspall, F. C., (1971). Error on Choroplethic Maps: Definition, Measurement, Reduction. *Annals of the Association of American Geographers*, Vol. 61(2), 217-244. https://doi.org/10.1111/j.1467-8306.1971.tb00779.x.

[30] Van Westen, C. J., Castellanos, E. and Kuriakose, S. L., (2008). Spatial Data for Landslide Susceptibility, Hazard, and Vulnerability Assessment: An Overview. *Engineering geology*, Vol. 102(3-4), 112-131. https://doi.org/10.1016/j.enggeo.2008.03.010.

[31] Tran, V. P., Duc, D. N. and Binh, T. P., (2023). Modeling and Mapping of Flood Susceptibility at Que Son District, Quang Nam Province, Vietnam Using Catboost. *IOP Conference Series.Materials Science and Engineering*, Vol. 1289(1). https://doi.org/10.1088/1757-899X/1289/1/012019.

[32] Nguyen, D., Chou, T., Hoang, T., and Chen, M. (2023). Flood Susceptibility Mapping Using Machine Learning Algorithms: A Case Study in Huong Khe District, Ha Tinh Province, Vietnam. *International Journal of Geoinformatics*, Vol. 19(7), 1–15. https://doi.org/10.52939/ijg.v19i7.2739.

[33] Islam, A. R. M. T., Talukdar, S., Mahato, S., Kundu, S., Eibek, K. U., Pham, Q. B., Kuriqi, A. and Linh, N. T. T., (2021). Flood Susceptibility Modelling Using Advanced Ensemble Machine Learning Models. *Geoscience Frontiers*, Vol. 12(3). https://doi.org/10.1016/j.gsf.2020.09.006.

[34] Sörensen, R., Zinko, U. and Seibert, J., (2006). On the Calculation of the Topographic Wetness Index: Evaluation of Different Methods Based on Field Observations. *Hydrology and Earth System Sciences*, Vol. 10(1), 101-112. https://doi.org/10.5194/hess-10-101-2006.

[35] Chapi, K., Singh, V. P., Shirzadi, A., Shahabi, H., Bui, D. T., Pham, B. T. and Khosravi, K., (2017). A Novel Hybrid Artificial Intelligence Approach for Flood Susceptibility Assessment. *Environmental Modelling & Software*, Vol. 95, 229-245. https://doi.org/10.1016/j.envsoft.2017.06.012.

[36] Yilmaz, O. S., (2022). Flood Hazard Susceptibility Areas Mapping Using Analytical Hierarchical Process (AHP), Frequency Ratio (FR) and AHP-FR Ensemble Based on Geographic Information Systems (GIS): A Case Study for Kastamonu, Türkiye. *Acta Geophysica*, Vol. 70(6), 2747-2769. https://doi.org/10.1007/s11600-022-00882-9.

[37] Samela, C., Albano, R., Sole, A. and Manfreda, S., (2018). A GIS Tool for Cost-Effective Delineation of Flood-Prone Areas. *Computers, Environment and Urban Systems*, Vol. 70, 43-52. https://doi.org/10.1016/j.compenvurbsys.2018.01.013.

[38] McFeeters, S. K., (1996). The Use of The Normalized Difference Water Index (NDWI) in the Delineation of Open Water Features. *International Journal of Remote Sensing*, Vol. 17(7), 1425-1432. https://doi.org/10.1080/01431169608948714.

[39] Shives, E., Chen, T. H. K. and Seto, K. C., (2025). Multiple Hazards and Exposure in California: A Space-Time Analysis of Temperature, Drought, and Wildfire. *International Journal of Disaster Risk Reduction*, Vol. 120. https://doi.org/10.1016/j.ijdrr.2025.105391.

[40] Qin, X., Wang, S., Meng, M., Long, H., Zhang, H. and Shi, H., (2025). Enhancing Urban Resilience through Machine Learning-Supported Flood Risk Assessment: Integrating Flood Susceptibility with Building Function Vulnerability. *npj Urban Sustainability*, Vol. 5(1). https://doi.org/10.1038/s42949-025-00208-w.

[41] Winsemius, H. C., Van Beek, L. P. H., Jongman, B., Ward, P. J. and Bouwman, A., (2013). A Framework for Global River Flood Risk Assessments. *Hydrology and Earth System Sciences*, Vol. 17(5), 1871-1892. https://doi.org/10.5194/hess-17-1871-2013.

[42] Rehak, D., Senovsky, P., Hromada, M., Lovecek, T. and Novotny, P., (2018). Cascading Impact Assessment in a Critical Infrastructure System. *International Journal of Critical Infrastructure Protection*, Vol. *22*, 125-138.

[43] Pamukçu Albers, P. and Evers, M., (2024). Assessing Flood Risk: Identifying Indicators and Indices for Period-Specific Flood Measures. *EGUsphere*, 1-29. https://doi.org/10.5194/egusphere-2024-2534.

[44] Usman Kaoje, I., Abdul Rahman, M. Z., Idris, N. H., Razak, K. A., Wan Mohd Rani, W. N. M., Tam, T. H. and Mohd Salleh, M. R., (2021). Physical Flood Vulnerability Assessment Using Geospatial Indicator-Based Approach and Participatory Analytical Hierarchy Process: A Case Study in Kota Bharu, Malaysia. *Water*, Vol. 13(13). https://doi.org/10.3390/w13131786.

[45] Englhardt, J., de Moel, H., Huyck, C. K., de Ruiter, M. C., Aerts, J. C. and Ward, P. J., (2019). Enhancement of Large-Scale Flood Risk Assessments Using Building-Material-Based Vulnerability Curves for An Object-Based Approach in Urban and Rural Areas. *Natural Hazards and Earth System Sciences*, Vol. 19(8), 1703-1722. https://doi.org/10.5194/nhess-19-1703-2019.

[46] Ghobadi, M. and Ahmadipari, M., (2024). Enhancing Flood Susceptibility Modeling: A Hybrid Deep Neural Network with Statistical Learning Algorithms for Predicting Flood Prone Areas. *Water Resources Management*, Vol. 38(8), 2687-2710. https://doi.org/10.1007/s11269-024-03770-7.

[47] Gorelick, N., Hancher, M., Dixon, M., Ilyushchenko, S., Thau, D. and Moore, R., (2017). Google Earth Engine: Planetary-Scale Geospatial Analysis for Everyone. *Remote sensing of Environment*, Vol. 202, 18-27. https://doi.org/10.1016/j.rse.2017.06.031.

[48] Ahmed, K. R. and Akter, S., (2017). Analysis of Landcover Change in Southwest Bengal Delta Due to Floods by NDVI, NDWI and K-Means Cluster with Landsat Multi-Spectral Surface Reflectance Satellite Data. *Remote Sensing Applications*: *Society and Environment,* Vol. 8, 168-181. https://doi.org/10.1016/j.rsase.2017.08.010.

[49] Thammaboribal, P., Tripathi, N., Lipiloet, S., and Mandadi, R. (2025). Flood Mapping and Damage Assessment Using UN-SPIDER Recommended Practices in Google Earth Engine: A Case Study of the 2024 Chiang Rai Flood, Thailand. *International Journal of Geoinformatics*, Vol. 21(3), 165–179. https://doi.org/10.52939/ijg.v21i3.4039.

[50] Alshammari, E., Rahman, A. A., Rainis, R., Seri, N. A. and Fuzi, N. F. A., (2023). The Impacts of Land Use Changes in Urban Hydrology, Runoff and Flooding: A Review. *Current Urban Studies*, Vol. 11(1), 120-141. https://doi.org/10.4236/cus.2023.111007.

[51] Amitrano, D., Di Martino, G., Di Simone, A. and Imperatore, P., (2024). Flood Detection with SAR: A Review of Techniques and Datasets. *Remote Sensing,* Vol. 16(4). https://doi.org/10.3390/rs16040656.

[52] Zhran, M., Ghanem, K., Tariq, A., Alshehri, F., Jin, S., Das, J., Pande, C. B., Pramanik, M., Hasher, F. F. B. and Mousa, A., (2024). Exploring a GIS-Based Analytic Hierarchy Process for Spatial Flood Risk Assessment in Egypt: A Case Study of the Damietta Branch. *Environmental Sciences Europe*, Vol. 36(184), 1-25. https://doi.org/10.1186/s12302-024-01001-9.

[53] Khan, T. U., Nabi, G., Ullah, S., Akbar, A., Omifolaji, J. K., Achakzai, J. K. and Iqbal, A., (2025). Mapping Flood Resilience: A Comprehensive Geospatial Insight into Regional Vulnerabilities. *Frontiers in Water*, Vol. 7. https://doi.org/10.3389/frwa.2025.1465505.

[54] De Brito, M. M. and Evers, M., (2016). Multi-Criteria Decision-Making for Flood Risk Management: A Survey of the Current State of the Art. *Natural Hazards and Earth System Sciences*, Vol. 16(4), 1019-1033. https://doi.org/10.5194/nhess-16-1019-2016.

[55] Yu, I., Park, K. and Lee, E. H., (2021). Flood Risk Analysis by Building Use in Urban Planning for Disaster Risk Reduction and Climate Change Adaptation. *Sustainability*, Vol. 13(23). https://doi.org/10.3390/su132313006.

[56] Mourato, S., Fernandez, P., Pereira, L. G. and Moreira, M., (2023). Assessing Vulnerability in Flood Prone Areas using Analytic Hierarchy Process—Group Decision Making and Geographic Information System: A Case Study in Portugal. *Applied Sciences*, Vol. 13(8). https://doi.org/10.3390/app13084915.

[57] D'Ayala, D., Wang, K., Yan, Y., Smith, H., Massam, A., Filipova, V. and Pereira, J. J., (2020). Flood Vulnerability and Risk Assessment of Urban Traditional Buildings in A Heritage District of Kuala Lumpur, Malaysia. *Natural Hazards and Earth System Sciences*, Vol. 20(8), 2221-2241. https://doi.org/10.5194/nhess-20-2221-2020.

[58] Nkonu, R. S., Antwi, M., Amo-Boateng, M. and Dekongmen, B. W., (2023). GIS-Based Multi-Criteria Analytical Hierarchy Process Modelling for Urban Flood Vulnerability Analysis, Accra Metropolis. *Natural Hazards*, Vol. 117(2), 1541-1568. https://doi.org/10.1007/s11069-023-05915-0.